A hybrid framework for the spin-up and initialization of distributed coupled ecohydrological-biogeochemical models

Taiqi Lian[1], Ziyan Zhang[2], Athanasios Paschalis[3,2], and Sara Bonetti[1]

[1]Laboratory of Catchment Hydrology and Geomorphology, École Polytechnique Fédérale de Lausanne (EPFL), 1951 Sion, Switzerland
[2]Department of Civil and Environmental Engineering, Imperial College London, UK
[3]Department of Civil and Environmental Engineering, University of Cyprus, Nicosia, Cyprus

Correspondence: Sara Bonetti (sara.bonetti@epfl.ch)

Abstract. Accurate initialization is a critical step in fully distributed ecohydrological and soil biogeochemical modeling applications, yet often hindered by the computational cost of achieving steady-state conditions across large spatial domains. This study presents a novel initialization framework that combines a flux-tracking 1D spin-up with a random forest (RF) algorithm to efficiently generate spatially heterogeneous and topography-informed initial conditions accounting for lateral fluxes of wa-

5   ter, carbon, and nutrients. The framework first performs a limited number of 1D simulations to obtain steady-state conditions in a subset of representative cells, then uses RF to extrapolate these results across the catchment. Applied to T&C-BG-2D, a fully coupled distributed ecohydrological-soil biogeochemical model, the scheme reconstructs spatial variability of soil carbon and nutrient patterns while reducing computational demands by up to 90% compared to a fully distributed spin-up procedure. A sensitivity analysis across multiple simulation scenarios reveals that the number of tracked cells required, varying from 20%

10   to 40% of total domain grid cells, depends on the catchment's spatial complexity and the environmental covariates embedded in the RF predictors. The framework developed here can be easily applied to other spatially distributed models and across diverse catchments, enabling large-scale distributed ecohydrological-biogeochemical model initializations under constrained computational budgets.

1   Introduction

15   Process-based ecohydrological and biogeochemical models have become widely used tools to study the cycling of water, carbon, and nutrients, and to predict ecosystem responses to anthropogenic and climatic changes. However, initialization remains a critical challenge in ecohydrological modeling (Thornton and Rosenbloom, 2005; Hashimoto et al., 2011), as initial conditions strongly influence model outputs and can substantially reduce the model's ability to predict short-term responses to climatic variability (e.g., Senarath et al., 2000). This issue becomes even more critical for models including soil biogeochemical compo-

20   nents and aiming to simulate the coupled dynamics of water, vegetation, and soil biogeochemistry (Thornton and Rosenbloom, 2005; Fatichi et al., 2019; Lian et al., 2025a). A common practice to specify initial conditions for model simulations is to run a model for a chosen time period until equilibrium (dynamic or steady state) is reached (Thornton and Rosenbloom, 2005; Seck et al., 2015). The duration of this spin-up process largely depends on the chosen initial state, the model parameters, and the

prescribed forcings (Thornton et al., 2002; Thornton and Rosenbloom, 2005; Shi et al., 2013). For hydrological models, this
25 stabilization period typically spans days to several years, depending on the variable of interest (e.g., Noto et al., 2008; Seck
et al., 2015; Kim et al., 2018; Baroni et al., 2019). In contrast, soil biogeochemical models often require much longer spin-up
periods, sometimes up to thousands of years (Randerson et al., 2009; Qu et al., 2018), to stabilize soil carbon and nutrient pools
and avoid unrealistic behavior caused by disequilibrium in biogeochemical fluxes (Thornton and Rosenbloom, 2005; Lugato
et al., 2014; Ammann et al., 2009; Nemo et al., 2017).

30 To reduce the computational burden of long spin-up periods, various strategies have been proposed for plot- or ecosystem-
scale models. Analytical solutions under simplified forcing conditions can be used for some terrestrial biosphere models (Zhan
et al., 2003; Xia et al., 2012; Qu et al., 2018; Schwarz et al., 2024). Thornton and Rosenbloom (2005) introduced several
acceleration techniques, including accelerated decomposition, nitrogen addition, and multivariate minimization, which reduced
spin-up time by up to 75% in the Biome-BGC model. Hashimoto et al. (2011) developed a "slow-relaxation scaling" method to
35 gradually adjust soil carbon and nitrogen pools, improving the stability and realism of spin-up in the CENTURY model. Other
approaches include performing spin-up of specific sub-modules only (Krinner et al., 2005), or integrating spin-up procedures
with data assimilation techniques to reduce computational demands across multiple sites (Ng et al., 2014). Table S1 presents
a non-exhaustive list of spin-up methods and their applications across coupled ecohydrological-soil biogeochemical models
applied at plot and ecosystem scales.

40 Model initialization is even more challenging in spatially distributed coupled ecohydrological-biogeochemical models (e.g.,
Tague and Band, 2004; Shi et al., 2018; Lian et al., 2025a), which require information on distinct soil carbon and nutrient pools,
whose spatial distribution is largely modulated by a combination of climatic, pedogenic, topographic, and biological landscape
attributes (Li et al., 2020; Lian et al., 2025a; Parvizi and Fatehi, 2025). Due to the scarcity of spatially explicit data on soil
biogeochemistry pools, most models apply uniform or averaged initial conditions, followed by a spin-up period (typically a few
45 years) to stabilize the system (e.g., Tague and Band, 2004; Zhang et al., 2018; Qiu et al., 2023). In the most extreme case, Chris-
tensen et al. (2008) applied a spatially distributed spin-up period of more than 2500 years to reach steady state conditions for
the soil carbon and nitrogen pools. However, the prolonged spin-up periods required for stabilizing the biogeochemical pools
can become computationally prohibitive when applied to thousands of grid cells. Moreover, existing initialization techniques,
often designed for plot-scale models or coarser spatial resolutions, are insufficient for spatially distributed systems, as they
50 neglect the effects of lateral transfers of water, carbon, and nutrients among computational cells in evaluating the long-term
steady state.

Recent advances in artificial intelligence and machine learning (ML) have provided new opportunities for environmental
modeling, including applications in hydrology, ecology, and soil science (e.g., Peters et al., 2007; Mahdavi et al., 2018; Tyralis
et al., 2019; Carranza et al., 2021; Gupta et al., 2021). In spatially distributed models with limited data availability, ML
55 methods, such as random forest (RF) approaches, offer a practical approach to estimate initial conditions. RF approaches
have been successfully applied in hydrology and soil science (e.g., for landcover classification, soil moisture estimation, and
mapping of soil hydraulic properties). These successes highlight its strong capability to extrapolate the spatial distribution
of soil carbon and nutrient pools based on a suite of environmental covariates, starting from a limited number of locations

with known steady-state conditions (Martin et al., 2014; Parvizi and Fatehi, 2025; Zeraatpisheh et al., 2022). In this context,
if steady-state conditions are known for a subset of grid cells, RF can be used to infer the spatial distribution of carbon and
nutrient pools across the entire catchment. However, a workflow for the effective use of RF approaches to initialize coupled
ecohydrological-biogeochemical models is currently not available.

The goal of this study is to develop a generalizable and computationally efficient methodology to initialize spatially distributed ecohydrological–biogeochemical models in complex catchments. Achieving this goal requires addressing three main
challenges: (i) the high computational demand of fully coupled spin-up procedures for soil carbon and nutrient pools, (ii)
the even greater computational costs of applying such spin-up in distributed 2D simulations, and (iii) the need for a strategy
that can be generalized across catchments with different levels of topographic complexity and soil and vegetation variability. To overcome these limitations, we propose a novel initialization scheme that combines a plot-scale flux-tracking spin-up
with a RF algorithm. The proposed spin-up procedure captures lateral transfers of water, carbon, and nutrients, while the RF
model uses well-established key controlling factors (i.e., topography, vegetation, and soil information) to reconstruct spatial
patterns of soil carbon and nutrient pools. We implement this framework in the recently developed fully distributed coupled
ecohydrological-soil biogeochemical model T&C-BG-2D (Lian et al., 2025a) and test the following hypotheses:

(H1) Spatially explicit spin-up is required to capture spatial variability in soil carbon and nutrient pools across a landscape;

(H2) Performing spin-up with lateral transport only at a subset of representative locations and extrapolating the results
statistically with a RF model provides sufficient accuracy;

(H3) The number of representative locations required depends on overall catchment heterogeneity as well as on the
specific predictors included in the RF model (e.g., additional soil or vegetation attributes);

(H4) Uncoupled spin-up simulations (soil biogeochemistry dynamics with constant vegetation fluxes) provide adequate
steady-state conditions for the model initialization.

To our knowledge, this is the first study to address initialization in a fully distributed coupled ecohydrological-soil biogeochemical model that mechanistically simulates coupled water, vegetation, and soil biogeochemical dynamics. The proposed
approach provides a flexible and computationally efficient solution to spatial initialization and can be readily adopted in other
modeling frameworks.

2 Materials and method

2.1 T&C-BG-2D model and study area

In this work, we use the recently developed coupled ecohydrological-soil biogeochemical model, T&C-BG-2D (Lian et al.,
2025a), to evaluate the effect of different initialization schemes on the spatial distribution of soil carbon and nutrient pools.

The original T&C model (Fatichi et al., 2012) simulates coupled water, energy, and carbon cycles at the land surface. It
includes modules for soil moisture dynamics and vegetation processes such as plant phenology, dynamic carbon allocation in
multiple plant carbon pools, and tissue turnover (Fatichi et al., 2012, 2016). The hydrological component simulates precipitation
interception, transpiration, evaporation, infiltration, and snow/ice hydrology. Soil water movement is represented using a quasi-
3D Richards equation, while surface water flow uses a kinematic wave approach (Paschalis et al., 2022). A soil biogeochemistry
component, T&C-BG (Fatichi et al., 2019), was integrated into the T&C model to simulate soil carbon and nutrient dynamics,
including nitrogen (N), phosphorus (P), and potassium (K). The biogeochemistry module partitions plant litter into pools
based on decomposability, and represents soil organic carbon (SOC) in three functional forms (mineral-associated, particulate,
and dissolved). Soil organic nitrogen (SON) dynamics are tightly coupled to carbon through stoichiometric C:N ratios. The
model simulates the temporal dynamics of SON, dissolved organic nitrogen (DON), and nitrogen stored in microbial and
macrofauna biomass. It also explicitly tracks inorganic nitrogen pools (ammonium (NH_4^+) and nitrate (NO_3^-)) whose dynamics
are regulated by mineralization, immobilization, biological uptake, leaching, volatilization, nitrification, and denitrification.
A comprehensive description of T&C-BG is available in Fatichi et al. (2019) and Botter et al. (2021). Recently, Lian et al.
(2025a) extended T&C-BG to a distributed framework (T&C-BG-2D) by explicitly accounting for lateral transport of water,
carbon, and nutrients between grid cells. The model explicitly considers the lateral transport of seven mobile carbon and
nutrient pools, including DOC, NH_4^+, NO_3^-, dissolved inorganic phosphorus (DIP), dissolved potassium ions (K^+), DON, and
dissolved organic phosphorus (DOP), considered as passive tracers transported following the water flow. Tracers are assumed
to be well-mixed in each storage compartment after vertical/lateral transport. At each hourly time step, the model updates
soil carbon and nutrient pools in each grid cell by accounting for laterally transported solutes, which in turn regulate local
vegetation dynamics. This enables the simulation of coupled ecohydrological-soil biogeochemical dynamics with the explicit
consideration of the role of topographic features and lateral transport in shaping spatio-temporal carbon and nutrient patterns
across a landscape.

The domain used to test and showcase the spin-up procedure in this study is the Erlenbach catchment (Fig. 1a), a 0.76 km²
basin in the central Swiss Pre-Alps (Stähli et al., 2021) where T&C-BG-2D has already been applied (Lian et al., 2025a). We
considered a spatial square grid resolution of 20 meters. Based on a previous application of T&C-BG-2D in this catchment
(Lian et al., 2025a), we used meteorological data to force the model covering a 9-year period (October 1, 2011 to September
30, 2020). During this time, the catchment received an average annual precipitation of 2200 mm, with a mean air temperature
of 6.5°C (Lian et al., 2025a). The spatial distribution of soil texture (here mostly loam and clay loam) was retrieved from Gupta
et al. (2024), and vegetation cover was obtained from Pazúr et al. (2021). As only one meteorological station (Erlenhöhe) is
available in Erlenbach, constant lapse rate values typical of the region were assumed. For example, we considered a constant
thermal lapse rate equal to -0.0045 °C/m (Nigrelli et al., 2018; Lian et al., 2025a). The Erlenbach catchment is a suitable study
area to showcase the spin-up and initialization procedure proposed here since model parameters have already been calibrated
and the area is relatively small (thus reducing the computational costs) but still with a highly pronounced topography. Specific
model settings and parameters for the simulations here can be found in Lian et al. (2025a).
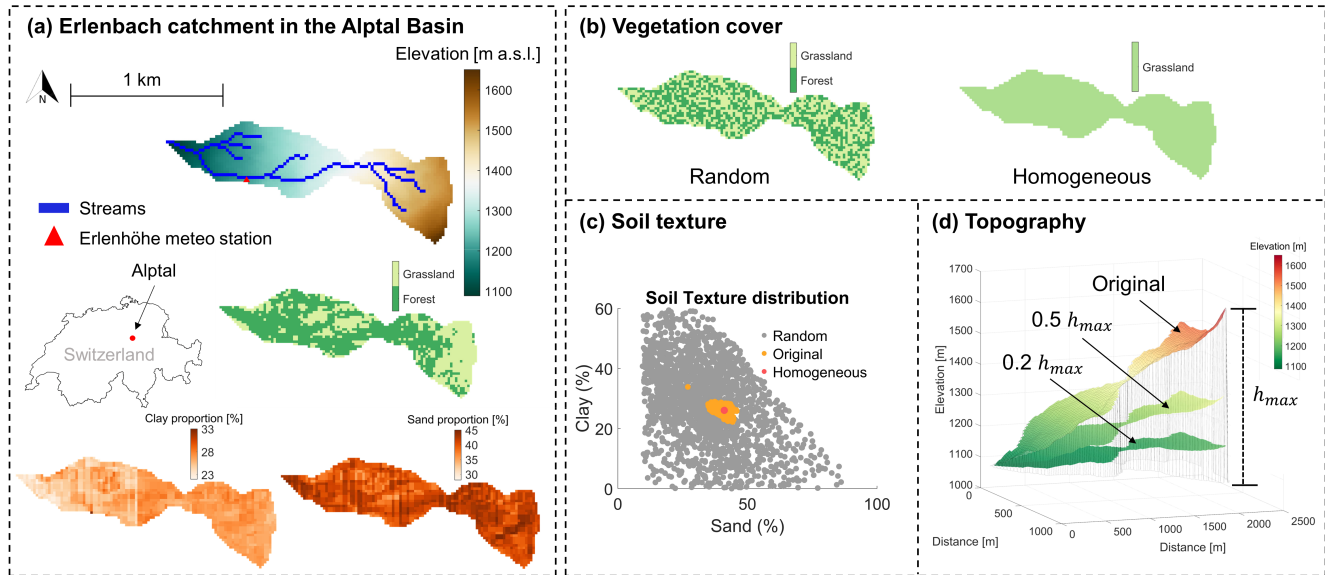
Figure 1. The Erlenbach catchment (a) and the modified catchment configurations (b-d) used to test the proposed initialization procedure. (a) Original catchment characteristics showing topography, stream network, vegetation cover, and sand and clay fractions. (b) Alternative vegetation scenarios: randomized grassland and forest cover (left), and homogeneous grassland (right). (c) Soil texture scenarios, represented in a sand–clay triangle: original soil texture (orange), randomized soil texture distribution (gray), and homogeneous soil texture (red). (d) Topographic scenarios generated by scaling the original digital elevation model by factors of 0.5 and 0.2.

2.2 Initialization procedure

The core strategy for the initialization framework proposed here involves two main steps: (1) performing a plot-scale spin-up in a limited number of selected cells while explicitly accounting for lateral fluxes of water, carbon, and nutrients, and (2) using a RF model to extrapolate the resulting steady-state pools across the entire model domain. A primitive version of this procedure was successfully applied in Lian et al. (2025a). However, no formal workflow was developed, and neither large-scale benchmarking nor a systematic sensitivity assessment of the method was conducted. In this study, we formalize the framework, evaluate its performance across multiple scenarios, and test its generality to enable seamless application in other models and study areas.

The scheme follows several steps, as shown in Fig. 2. First, a plot-scale simulation using T&C model is run for each soil–vegetation combination to obtain climatologically driven, nutrient-unstressed water and vegetation fluxes (dashed box in Fig. 2a). Then, we run the T&C-BG biogeochemistry module to reach a steady state (Fig. 2a) using the long-term average meteorological inputs and averaged water and vegetation fluxes (from T&C model). The resulting steady-state carbon and nutrient pools are then uniformly assigned to all cells with the same land cover type, resulting in spatially homogeneous initial conditions for each soil–vegetation combination (see Fig. 2b for an example in the Erlenbach catchment). Ideally, one should
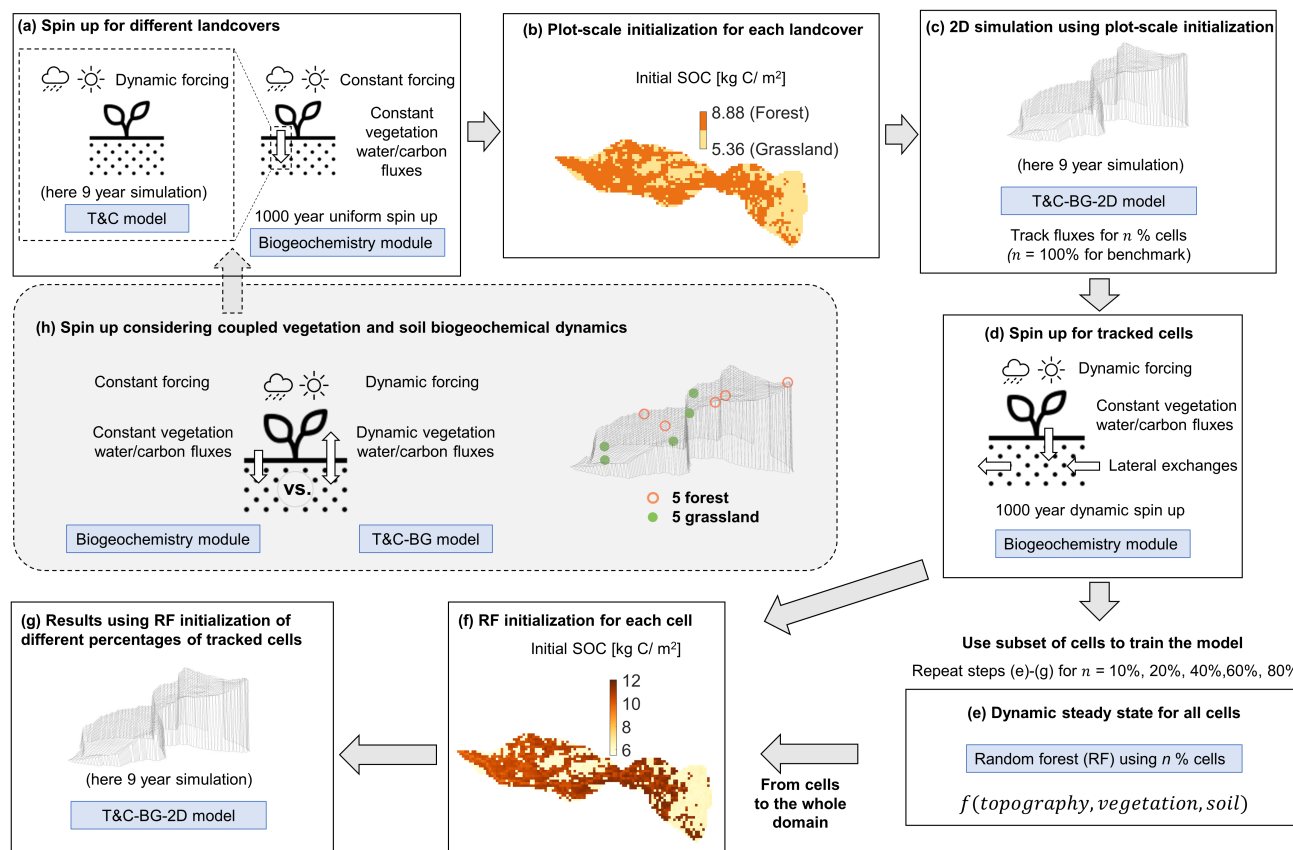
Figure 2. Workflow of the model initialization procedure. (a) For each soil–vegetation combination, perform T&C model to get averaged water and plant fluxes, which are used in a 1D spin-up via the T&C-BG biogeochemistry module using long-term average meteorological inputs. The resulting steady-state pools are then assigned to all cells with the same soil–vegetation combination (b). (c) A 2D simulation (T&C-BG-2D) is run with these initial conditions, tracking fluxes for a given percentage n of all grid cells. (d) For these cells, T&C-BG biogeochemistry module 1D spin-up with dynamic meteorology and imposed lateral fluxes is run to achieve a dynamic steady state in all tracked cells. (e) A random forest (RF) model is trained on results from different percentages of the subset of these cells (n) using topographic, soil, and vegetation attributes as predictors to reconstruct the initial conditions for the entire catchment domain (f), which are then used to initialize the final simulations (g). For each simulation scenario, steps (e) to (g) are repeated for different percentages of tracked cells n to investigate the optimal number of cells for the RF algorithm. (h) Additional plot-scale simulations are performed for 10 representative cells (5 forest, 5 grassland) to obtain a reference steady state using the fully coupled T&C-BG model (i.e., also considering dynamic vegetation fluxes), which is compared to the initial states generated in step (a).

perform this step for each major vegetation and soil type combination. For the application here, given the limited variability in soil texture across the catchment, the averaged soil texture was considered. Next, a 2D simulation is performed using the initial conditions obtained from step b (Fig. 2c). In this simulation, lateral biogeochemical fluxes are tracked (i.e., lateral

140 fluxes of DOC, NH_4^+, NO_3^-, DIP, K^+, DON, and DOP) across all grid cells in the domain. Note that, in this step, available spatially variable information on soil texture (Gupta et al., 2024) is used. The soil biogeochemistry module is then run using dynamic meteorological forcing (here repeating the 9 years of data available), incorporating the tracked lateral exchanges, until a dynamic steady state is reached (Fig. 2d). The flux-tracking step (c) captures the influence of topography, although we should note that soil carbon and nutrient pools respond slowly to spatial gradients and may not fully equilibrate within a

145 short simulation period. In the 2D simulation in Fig. 2c, ideally, the entire available forcing period should be used to capture representative vegetation dynamics and to track biogeochemical fluxes as accurately as possible. In this case, the 9-year data were used, but a longer simulation would provide a more robust basis for the subsequent spin-up of the biogeochemical pools. A sensitivity analysis comparing the dynamic steady state of the biogeochemical pools using different lengths of tracking fluxes is presented in Fig. S1. Using only 1 year for the 2D simulation in step (c) introduced a bias of 3% in the steady-state SOC in

150 grassland areas in step(d) compared to using all 9 available years.

The case in which lateral fluxes are tracked in $n = 100\%$ of the cells is considered here as a benchmark. In this case, the dynamic steady-state conditions from all grid cells are directly used as the initial state for a subsequent 9-year simulation (from Fig. 2d to Fig. 2f). This approach provides the highest accuracy, as each cell undergoes its own spin-up process while accounting for lateral fluxes and topographic variability. However, such a comprehensive spin-up is computationally demanding

155 and should not be repeated for every new case study, as it would undermine the purpose of an efficient initialization protocol. Our objective is therefore to identify the minimum fraction of tracked cells n needed to approximate this benchmark with acceptable accuracy. To this purpose, a RF model (Loh, 2002; Breiman, 2001) is trained using a subset of tracked cells n (equal to 10%, 20%, 40%, 60%, or 80%) to predict the spatial distribution of soil carbon and nutrient pools across the domain (Fig. 2e). The covariates used as predictors include topographic features (elevation, slope, drainage area, and profile curvature),

160 soil properties (percentage of sand), and vegetation type (forest or grassland). The steady-state pools predicted by the RF (Fig. 2f) are then used to initialize the final simulation over the period of interest (here 9 years, Fig. 2g). Because the distributions of topographic, soil, and vegetation characteristics across the full domain are known in advance, the selected training cells were chosen to preserve these distributions and thus ensure representativeness (Fig. S2).

The performance of different initialization schemes (i.e., without RF ($n = 0\%$) and with $n < 100\%$) is assessed by com-

165 paring the spatial distributions of soil carbon and nutrient pools — specifically SOC, DOC, and SON — with those from the benchmark case ($n = 100\%$). First, simulations without RF or dynamic lateral fluxes (the direct output of step (c) in Fig. 2) are compared with the benchmark to address hypothesis H1, testing the need for spatially-informed spin-up to capture carbon and nutrient spatial variability. Second, RF-initialized simulations are compared with the benchmark to address H2, thus evaluating whether extrapolation from a subset of representative cells can reasonably approximate the benchmark while reducing the

170 computational requirements.

A sensitivity analysis was also performed to assess the relative importance of individual predictors in the RF algorithm. The six predictors considered were elevation, slope, flow accumulation area, profile curvature, percentage of sand, and vegetation type. Each predictor was individually removed from the RF training process using $n = 40\%$ tracked cells under the original simulation scenario (see other simulation scenario in Section 2.3). For each reduced predictor set, a new RF model was trained,

175 and its ability to reconstruct the spatial patterns of carbon and nutrient pools was compared against the full model (with all six covariates). This analysis provides insight into the relative influence of individual predictors and helps us to assess how predictor choice may affect the sampling requirements (hypothesis H3).

2.3 Design and analysis of different catchment configurations

In addition to the original simulation scenario (hereafter *Original*), a set of modified simulation setups was designed to evaluate
180 the generality of the proposed initialization method and to assess its performance under varying levels of landscape complexity. Each simulation scenario introduces a targeted modification to one aspect of the catchment configuration, while keeping all other properties unchanged:

- Vegetation cover (Fig. 1b): the existing vegetation is replaced either with a randomized spatial distribution while maintaining the original forest-to-grassland ratio (*Random Veg*), or with a uniform grassland cover across the entire domain
185 (*Homog. Veg*).

- Soil texture (Fig. 1c): the original soil texture map is replaced either with a randomized spatial distribution (*Random Soil*, gray points in Fig. 1c) or with a uniform soil texture across the domain (*Homog. Soil*, red point in Fig. 1c).

- Topography (Fig. 1d): this is modified by reducing the elevation of the highest point by factors of 0.5 and 0.2 (0.5 h_{max} and 0.2 h_{max}), while keeping the lowest elevation fixed and adjusting all intermediate elevations proportionally.
190 As T&C-BG-2D uses spatially distributed meteorological inputs derived from a fixed station and lapse rates, a flatter topography necessarily results in more spatially uniform meteorological forcings in these simulation scenarios. Note that the elevation of the meteorological station was also rescaled in these two simulation scenarios.

In all cases, only one factor is varied per simulation scenario (i.e., vegetation, soil, or topography), while the remaining inputs are kept consistent with the *Original* simulation setup. For each scenario, the full initialization sequence described in
195 Fig. 2 (steps a–g) is applied, with different RF initialization settings based on the percentage of tracked cells n (steps e–g). For clarity, simulations are denoted as $n\%$, where n indicates the percentage of tracked cells used in the RF initialization ($n = 0$, 10, 20, 40, 60, 80, or 100). $n = 0\%$ corresponds to simulations applying initial conditions from the 1D spin-up without RF or dynamic lateral fluxes (the direct output of step c in Fig. 2), while $n = 100\%$ represents simulations in which lateral fluxes in all cells are tracked.

200 For the soil texture and topography scenarios, results for n equal to 60% and 80% are omitted, as a satisfactory performance was already achieved with $n = 40\%$ of tracked cells. Note that, for the analysis related to soil texture, in step (a) of the procedure (see Fig. 2) the average soil texture is used, while spatial variability in soil textural properties is only taken into account from step (c) onward. The implications of this assumption were investigated with additional dedicated numerical tests and are discussed in the discussion section. Overall, the design of these scenarios allows us to evaluate how vegetation, soil,
205 and topographic heterogeneity may affect the number of representative locations required for RF initialization (hypotehsis H3).

2.4 Steady state with coupled vegetation dynamics

In steps (a) and (d) of the initialization workflow (Fig. 2), vegetation fluxes are held constant and only the biogeochemistry module is used for spin-up. This decoupling strategy further reduces computational costs, as instead of solving the full system of coupled ordinary differential equations, the model reduces to a single biogeochemical system that can be solved at minimal

210   computational cost. Such an approach is commonly used to approximate near-equilibrium states in terrestrial biosphere models (Krinner et al., 2005). To evaluate the effect of neglecting vegetation dynamics during spin-up, we selected five cells for each vegetation type (forest and grassland) across a range of topographic conditions. For each selected cell, we compared the resulting steady state from the decoupled spin-up (using only the biogeochemistry module) to the steady state obtained from the fully coupled T&C-BG model, simulating the long-term vegetation-soil biogeochemistry dynamic (Fig. 2h). Details on the

215   selected cells are provided in Fig. S2 and Table S2. For the fully coupled T&C-BG model, the repeated 9-year meteorological data are used to force the model, and the simulations were initialized using the soil carbon and nutrient pools from step (b) in Fig. 2. For every 9-year simulation, the long-term trend of all simulated soil carbon and nutrient pools was evaluated, using singular spectrum analysis to exclude interannual seasonalities. The steady state was considered reached when the trends of all soil carbon and nutrient pools changed by less than 1% simultaneously during a 9-year simulation. Then, the average of the

220   final 3-year simulation periods was adopted and compared to results from the uncoupled dynamics using the biogeochemistry module with constant vegetation fluxes. This numerical experiment was specifically designed to address hypothesis H4, testing whether uncoupled spin-up simulations provide adequate steady-state conditions compared to the fully coupled case.

3 Results

3.1 Effect of different initialization settings on the spatial distribution of carbon and nutrient pools

225   Fig. 3 shows the spatial distribution and associated probability density functions (PDFs) of 9-year averaged SOC, DOC, and SON (step (g) in Fig. 2) under the *Original* setup. Results are shown for the benchmark simulation ($n = 100\%$), the 2D simulation applying initial condition from 1D spin-up without RF or dynamic lateral fluxes ($n = 0\%$, direct output of step (c) in Fig. 2), and RF-based initializations using different percentages of tracked cells n (see also Fig. S3 for additional results). Compared to the $n = 0\%$ simulation, which neglects long-term topographic effects on soil biogeochemistry dynamics from

230   initial conditions, the benchmark case exhibits greater spatial variability in SOC and SON, highlighting the role of topography in shaping soil carbon and nutrient distributions. In contrast, the spatial distribution of DOC (a small fraction of SOC) remains nearly identical between the benchmark and all initialization settings, regardless of the percentage of tracked cells considered. This is likely due to the fact that DOC is rapidly transported by water and its spatial variability is largely captured during the 9-year simulation, even without dynamic spin-up or RF-based initialization. Since the spatial performance of DOC is

235   satisfactory even without RF, subsequent analyses and results presented here will focus on SOC and SON only. The PDFs of SOC and SON (Fig. 3) further indicate that the $n = 0\%$ simulation underestimates both the spatial variability and median values. This bias arises because the $n = 0\%$ simulation uses steady-state conditions from a single location (the meteorological
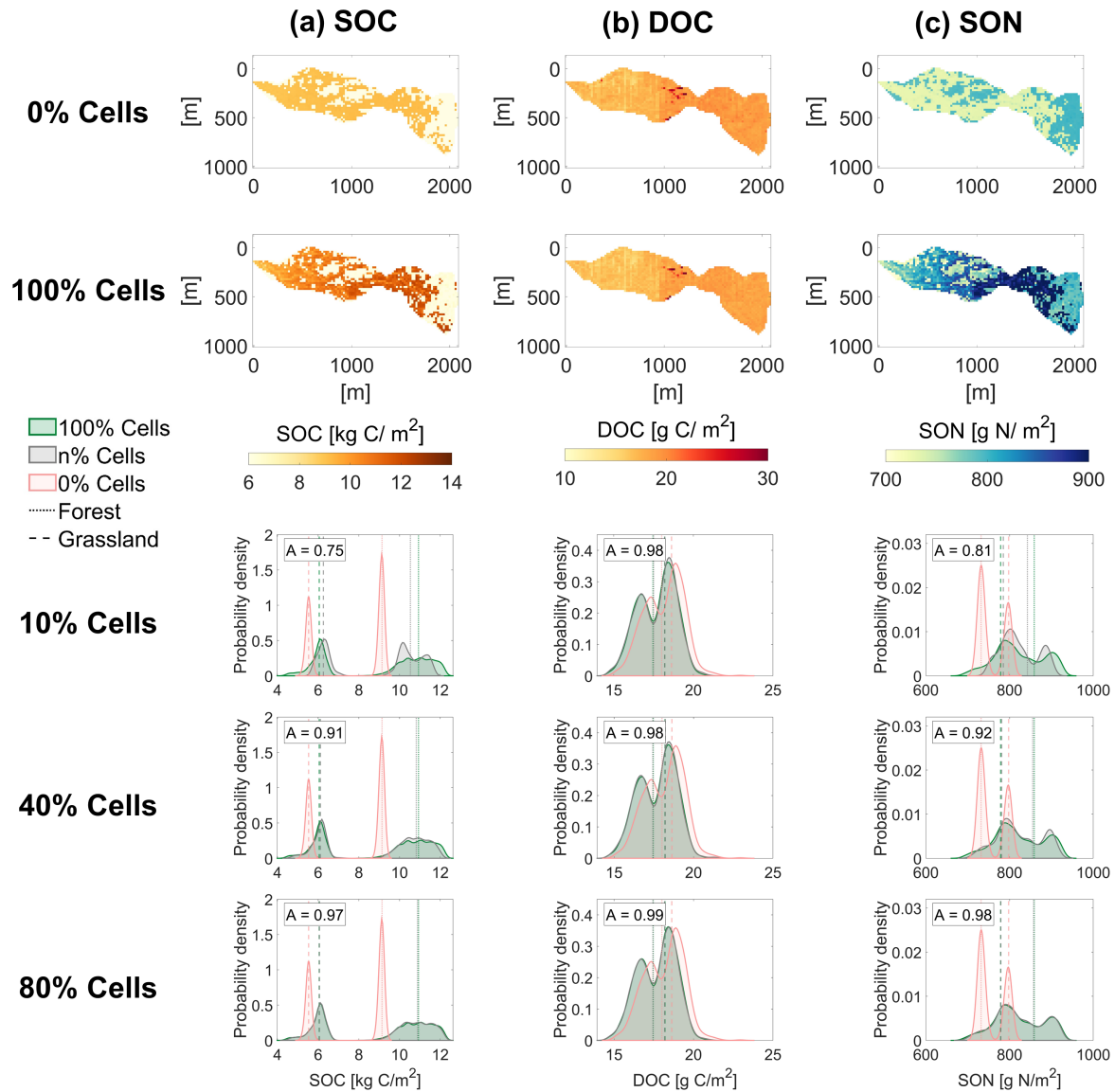
Figure 3. Spatial distributions of (a) soil organic carbon (SOC), (b) dissolved organic carbon (DOC), and (c) soil organic nitrogen (SON) in the Erlenbach catchment with the *Original* setup under two initialization conditions: with 0% cell tracking (0% Cells) and with 100% cell tracking (100% Cells). Probability density functions (PDFs) of each variable are shown for simulations using RF initialization with $n = 10\%$, 40%, and 80%. Each is compared to the corresponding PDFs from the 0% cells and 100% cells simulations. The overlap area between PDFs (A value) is used to quantify the similarity between the RF-based distributions and the benchmark. Dashed and dotted lines represent median values for grassland and forest areas, respectively.

Table 1. Overlap area (A value) between the probability density functions (PDFs) of soil organic carbon (SOC) and soil organic nitrogen (SON) from different percentages of tracked cells and those from the benchmark simulation across multiple simulation scenarios. Values in parentheses under the *Random Soil* scenario represent results obtained when clay content was included as an additional predictor in the random forest model. Values greater than or equal to 0.90 are shown in bold.

Scenarios/Track cells [%]		10	20	40	60	80
Original	SOC	0.75	0.82	**0.91**	**0.95**	**0.97**
	SON	0.81	0.86	**0.92**	**0.96**	**0.98**
Random Veg	SOC	0.80	0.83	**0.92**	**0.94**	**0.97**
	SON	0.84	0.87	**0.92**	**0.96**	**0.98**
Homog. Veg	SOC	0.83	**0.91**	**0.94**	**0.97**	**0.98**
	SON	0.83	**0.91**	**0.92**	**0.95**	**0.98**
Random Soil	SOC	0.58 (0.85)	0.68 (**0.90**)	0.76 (**0.95**)		
	SON	0.65 (0.88)	0.74 (0.89)	0.80 (**0.96**)		
Homog. Soil	SOC	0.74	0.85	**0.92**		
	SON	0.82	**0.90**	**0.95**		
0.5 h_{max}	SOC	0.72	0.82	**0.91**		
	SON	0.75	0.85	**0.91**		
0.2 h_{max}	SOC	0.77	0.82	**0.91**		
	SON	0.83	0.87	**0.93**		

station), which would require much longer simulation time to reflect the effects of heterogeneous environmental conditions and lateral exchanges (see more details in Section 3.3). Note that the bimodality of the PDFs arises from the two different types of
240 vegetation cover in the catchment.

Interestingly, RF initialization using just $n = 10\%$ of the cells can reproduce approximately 75% of the spatial variability in SOC (Fig. 3). Model performance improves with increasing percentages of tracked cells, and using $n = 80\%$ yields results that are nearly indistinguishable from the benchmark simulation. A notable performance jump occurs between $n = 20\%$ and 40%: for example, in the *Original* simulation scenario, the overlap area (A value, quantifying the overlap between the PDFs of each
245 simulation and the benchmark and a value of A close to 1 indicates high similarity between distributions) increases from 0.82 to 0.91 for SOC and from 0.86 to 0.92 for SON (Table 1). Considering A $\geq$ 0.9 as a threshold for satisfactory performance yields $n = 40\%$ of tracked cells being sufficient to accurately capture most of the spatial variability in SOC and SON (see Table 1) for the original Erlenbach simulation scenario. The other metric (Jensen–Shannon divergence) comparing similarities between PDFs is reported in Table S3. However, the optimal percentage of tracked cells may vary depending on catchment
250 characteristics such as vegetation composition, soil texture, topographic complexity, and background climate (see Section 3.2).
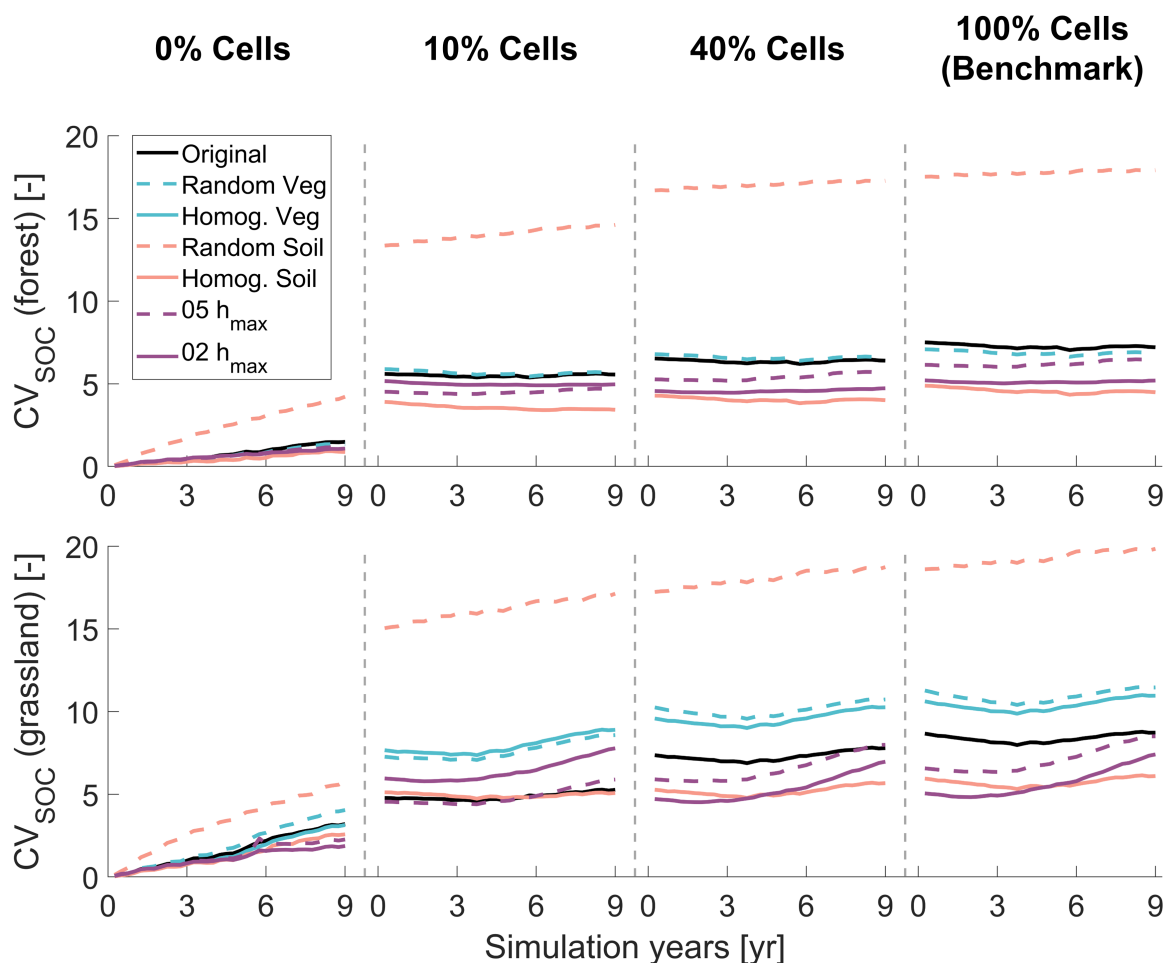
Figure 4. Temporal evolution of the coefficient of variation (CV) of soil organic carbon (SOC) over a 9-year simulation period in forest (top) and grassland (bottom) under different initialization settings and simulation scenarios. Each column represents one initialization setting: no cells tracking and no random forest ($n = 0\%$), $n = 10\%$ cells tracking and random forest (10% Cells), $n = 40\%$ cells tracking and random forest (40% Cells), and $n = 100\%$ cells tracking (100% Cells). Line colors and styles indicate results from different simulation scenarios, as shown in the legend.

Black lines in Fig. 4 show the temporal evolution of the coefficient of variation (CV, defined as the ratio of standard deviation to the mean) for spatial SOC under different RF initialization settings in forested and grassland areas (corresponding results for SON are provided in Fig. S4). In the $n = 0\%$ initialization, CV increases steadily over the 9-year simulation, indicating that spatial variability has not reached a steady state. In contrast, simulations initialized using the RF scheme maintain relatively 255 stable CV values throughout the simulation period, with variability reflecting responses to dynamic environmental drivers rather than spin-up imbalance. CV values gradually increase across RF initialization settings with higher tracking percentages

(n), approaching those of the benchmark. Notably, CV trajectories for RF settings using $n = 40\%$ and 100% of tracked cells are nearly identical, confirming that $n = 40\%$ is sufficient to reproduce the full temporal dynamics of SOC spatial variability in the catchment here. These results provide direct support for H1, demonstrating that spatially explicit initialization is required to capture spatial variations of SOC and SON, as well as for H2, showing that spin-up at a subset of representative locations combined with RF extrapolation can satisfactorily reproduce benchmark dynamics.

3.2 Sensitivity across different catchment configurations

Table 1 and Fig. 4 also report the performance of using different n values in the RF model across different catchment configurations. Across all simulation scenarios, $n = 40\%$ can capture over 90% of the spatial variability in both SOC and SON. An exception is observed in the *Homog. Veg* simulation scenario, where even $n = 20\%$ of tracked cells yields satisfactory performance.

A comparison among *Original*, *Random Veg*, and *Homog. Veg* simulations suggests that the number of tracked cells required for satisfactory RF performance is more sensitive to the proportion of vegetation types than to their spatial arrangement. As expected, when vegetation cover is spatially homogeneous, fewer cells are needed to achieve accurate predictions.

In contrast, results from the *Original*, *Random Soil*, and *Homog. Soil* simulations indicate that reducing the spatial heterogeneity of soil texture lowers the absolute spatial variability of SOC but does not necessarily reduce the number of tracked cells required for RF initialization. This is likely because soil texture is already included as a predictor in the RF model, and because, in the *Original* scenario soil texture is relatively uniform (i.e., sand content: mean = 41%, standard deviation = 2% based on Gupta et al. (2024)). As a result, the model can capture soil-related variability effectively without the need for additional soil information. However, in the *Random Soil* scenario, where soil texture is highly heterogeneous, adding supplementary predictors such as the percentage of clay significantly improves the model's ability to reproduce benchmark SOC spatial patterns (Table 1). This highlights the importance of including sufficient soil information when simulating spatial variability under heterogeneous soil conditions. These findings are consistent with previous studies showing that soil properties are among the most influential predictors in digital soil mapping of SOC (e.g., Meersmans et al., 2008; Zeraatpisheh et al., 2022; Martín-López et al., 2023).

Simulation results from the flatter topography scenarios (0.5 h_{max} and 0.2 h_{max}) indicate that a more gentle topography does not necessarily lower the number of tracked cells needed for accurate RF initialization. In general, RF models require more samples when predictor distributions are not evenly distributed within their overall range of variation (e.g., when extreme values are underrepresented), in order to adequately represent the edges and tails of the input space (Peters et al., 2007; Simon et al., 2023). In our sampling design, the distributions of predictor variables were known in advance, and the selected cells were chosen to represent the full range of topographic and land cover features across the domain (Fig. S2). This targeted selection likely contributed to consistent RF performance across topographic conditions. It is also important to note that, in these simulations, the use of flatter topographies only results in reduced elevation differences, slopes, and curvatures, without altering the overall catchment shape, size, and contributing area, as the underlying catchment skeleton remains identical across scenarios. Additionally, the topographies were modified by tilting the surface around the lowest elevation point. This alters

the temperature regime and introduces a bias in SOC compared to the original simulation. While this can affect the average temperature values in the domain (and resulting absolute values of SOC and SON), it has no impact on the number of cells required within the same simulation configuration. Overall, these results highlight that the number of representative locations needed for satisfactory RF initialization is shaped by catchment-specific heterogeneity and predictor distributions, thereby
295   supporting H3.
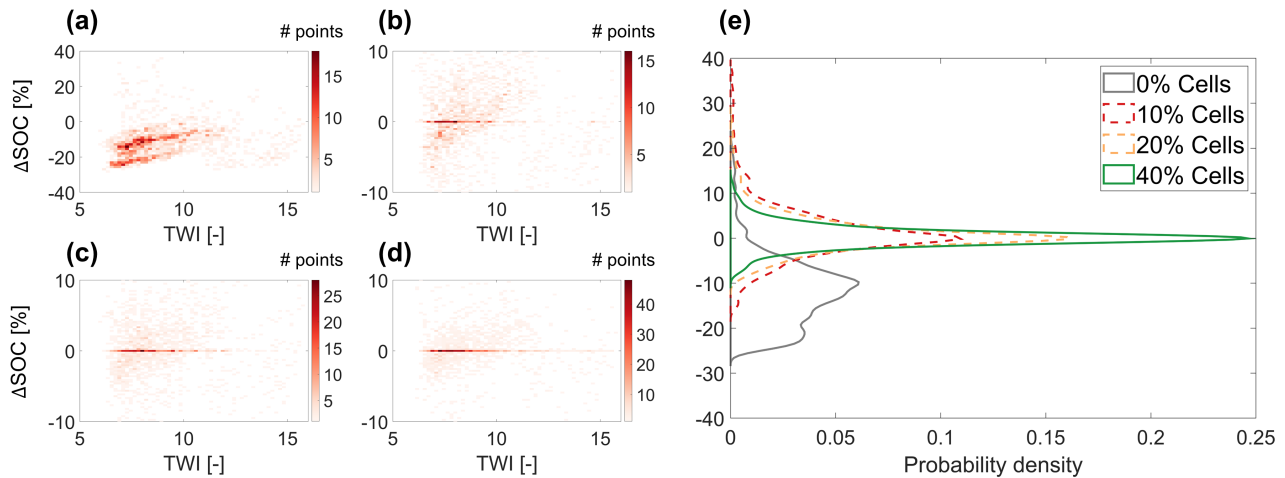
Figure 5. Density maps showing the relationship between relative SOC bias ($\Delta SOC = (SOC_{\text{simulation}} - SOC_{\text{benchmark}})/SOC_{\text{benchmark}}$) and Topography Wetness Index (TWI) under *Original* simulation scenarios with $n =$ (a) 0%, (b) 10%, (c) 20%, and (d) 40%. (e) Probability density functions (PDFs) of ΔSOC from $n = 0\%$ (in gray), and with RF-based initialization using $n = 10\%$ (red dashed line), 20% (yellow dashed line), and 40% (green) of tracked cells.

3.3   Bias analysis in relation to topography

Fig. 5 presents the relationship between relative SOC bias ($\Delta SOC = (SOC_{\text{simulation}} - SOC_{\text{benchmark}})/SOC_{\text{benchmark}}$) and the topographic wetness index (TWI) from the *Original* simulation scenarios with $n = 0\%$, 10%, 20%, 40% and the PDF of ΔSOC. Additional results covering all simulation scenarios are provided in Figs. S5-S6.

300   Fig. 5a shows that the $n = 0\%$ initialization configuration results in a systematic underestimation of SOC in many cells, with deviations reaching up to 20–30% in some cases. This is because the initial pools (Fig. 2b) are derived from the 1D spin-up at the Erlenhöhe meteorological station, located at a relatively low elevation (1210 m a.s.l.) within the catchment. Since SOC generally increases with elevation due to temperature reductions (Parras-Alcántara et al., 2015; Teng et al., 2017; Zhu et al., 2019) – an effect captured by T&C-BG-2D (Lian et al., 2025a) – SOC in high-elevation areas gradually accumulates over time.
305   However, the 9-year $n = 0\%$ simulation is insufficient for these areas to equilibrate, leading to a consistent underestimation (compared to the benchmark simulation, which instead captures the increasing trend of SOC with elevation) due to the lack of spatial information in the model initialization.

(a)

(b)

(c)

(d)
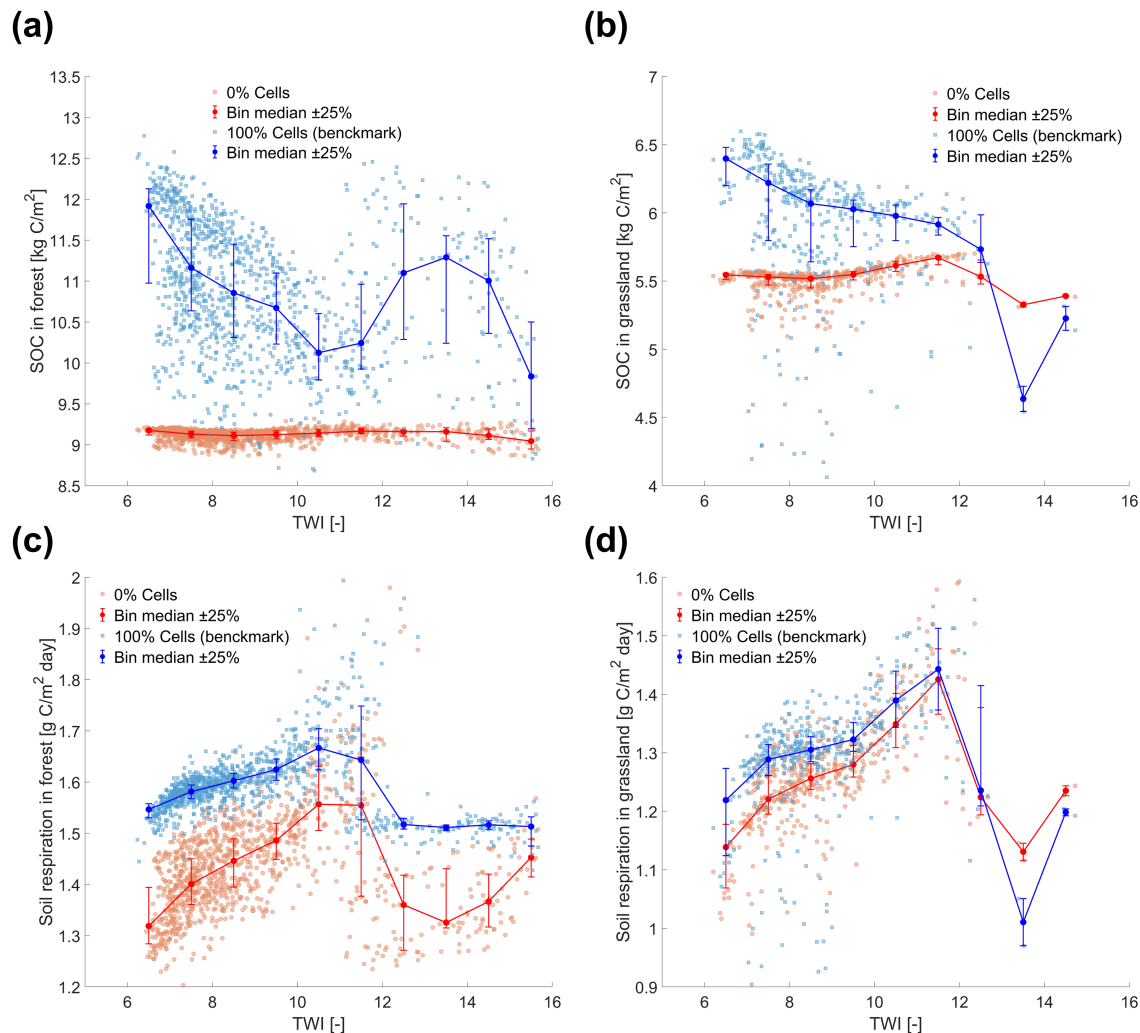
Figure 6. Relationship between the topographic wetness index (TWI) and (a, b) soil organic carbon (SOC) and (c, d) soil respiration in the *Original* simulation scenario, shown separately for forest (left) and grassland (right). Red points and lines represent results from $n = 0\%$ simulations; blue squares and lines show results from $n = 100\%$ simulations. Filled circles indicate the median values within TWI bins of width 1, with vertical bars showing the $\pm 25\%$ range within each bin.

Interestingly, a positive relationship between ΔSOC and TWI is observed in the range TWI < 11, where the majority of grid cells are located (Fig. 5a). This trend can be explained primarily by the influence of water availability on soil respiration and, consequently, on SOC stocks. We note, however, that TWI is weakly but significantly correlated with elevation, and thus with air temperature ($r = -0.14$, $p < 0.05$). This suggests that temperature may also contribute to the observed relationship, although its influence is relatively minor compared to that of water availability. When the $n = 0\%$ initialization is applied,

SOC exhibits almost no trend with TWI (Fig. 6a,b). However, the benchmark simulation shows a decreasing SOC trend with increasing TWI for TWI < 11, reflecting a long-term steady-state pattern shaped by soil respiration processes during spin-

315   up. This is consistent with previous findings that soil respiration increases with water availability due to enhanced microbial activity (Manzoni et al., 2012, 2014; Yan et al., 2018), as shown in Fig. 6c,d. However, under excessively wet conditions (such as, TWI > 11), this relationship reverses due to oxygen limitation (Moyano et al., 2013; Ruiz et al., 2015). Because the SOC distribution in the benchmark simulation shows much higher spatial variability than in the $n = 0\%$ case, the decreasing SOC–TWI trend from the benchmark dominates the $\Delta SOC - TWI$ relationship, leading to an apparent positive correlation

320   in Fig. 5a. The PDFs in Fig. 5e further confirm that the RF initialization scheme substantially reduces this topography-related bias. Using only $n = 10\%$ of the cells for RF training already eliminates most of the systematic bias (Fig. 5b), while $n = 20\%$ (Fig. 5c) and $n = 40\%$ (Fig. 5d) eliminates it almost entirely.

3.4   The role of coupled vegetation dynamics in 1D soil biogeochemical spin-up

Fig. 7 compares SOC values obtained from different simulation stages and spin-up strategies. The first column represents the

325   initial SOC values (here, values in Fig. 2b are used, but can be derived from steady state in areas with similar land cover, soil, and climatic conditions, or a reasonable initial guess). The next three columns show SOC values after 9, 18, and 27 years of simulation using the full T&C-BG model (i.e., with coupled soil biogeochemical and vegetation dynamics). The gray box in the middle shows the SOC state obtained using the biogeochemistry-only spin-up with 9-year average vegetation fluxes after 1000 years (i.e., no coupled vegetation dynamics - equivalent to step (a) in Fig. 2). Starting from this uncoupled spin-up steady

330   state, an additional 27 years of simulation (3 × 9 years) were performed using the full T&C-BG model, with results shown in the three subsequent central columns. The red box on the far right indicates the reference steady state achieved through long-term simulation with the fully coupled T&C-BG model, which considers the coupled vegetation-soil biogeochemistry dynamics. Each boxplot includes five representative sites with different vegetation types (see Fig. 2h). Site-specific vegetation and soil information, along with SOC and SON pool sizes, are provided in Table S2. A corresponding analysis for SON is

335   shown in Fig. S7.

As shown in Fig. 7, the initial SOC values are substantially underestimated in the case here and gradually increase over the course of the simulation. After a 27-year simulation period with the fully coupled T&C-BG model, the resulting SOC is still largely underestimated compared to the long-term steady state (red shading). Reaching steady state with the fully coupled model would require approximately 1000 years. A direct comparison of SOC between the uncoupled spin-up steady state (mid-

340   dle gray box in Fig. 7) and the reference steady state from the fully coupled plot-scale spin-up (red shading) reveals an average underestimation of 19.2% and 10.6% for grassland and forested sites, respectively (see also Table S2). This underestimation is further reduced for the case of SON (see Fig. S7). This uncoupled spin-up steady state can be reached by first running the fully coupled model for only a short period (here 9 years) to obtain average vegetation fluxes, which are then used to drive the biogeochemistry-only spin-up. This provides a substantial gain in computational efficiency despite the slight disagreement in

345   steady states, thus supporting the choice of adopting an uncoupled spin-up approach as a first step (Fig. 2a) within the proposed initialization framework and confirming H4..
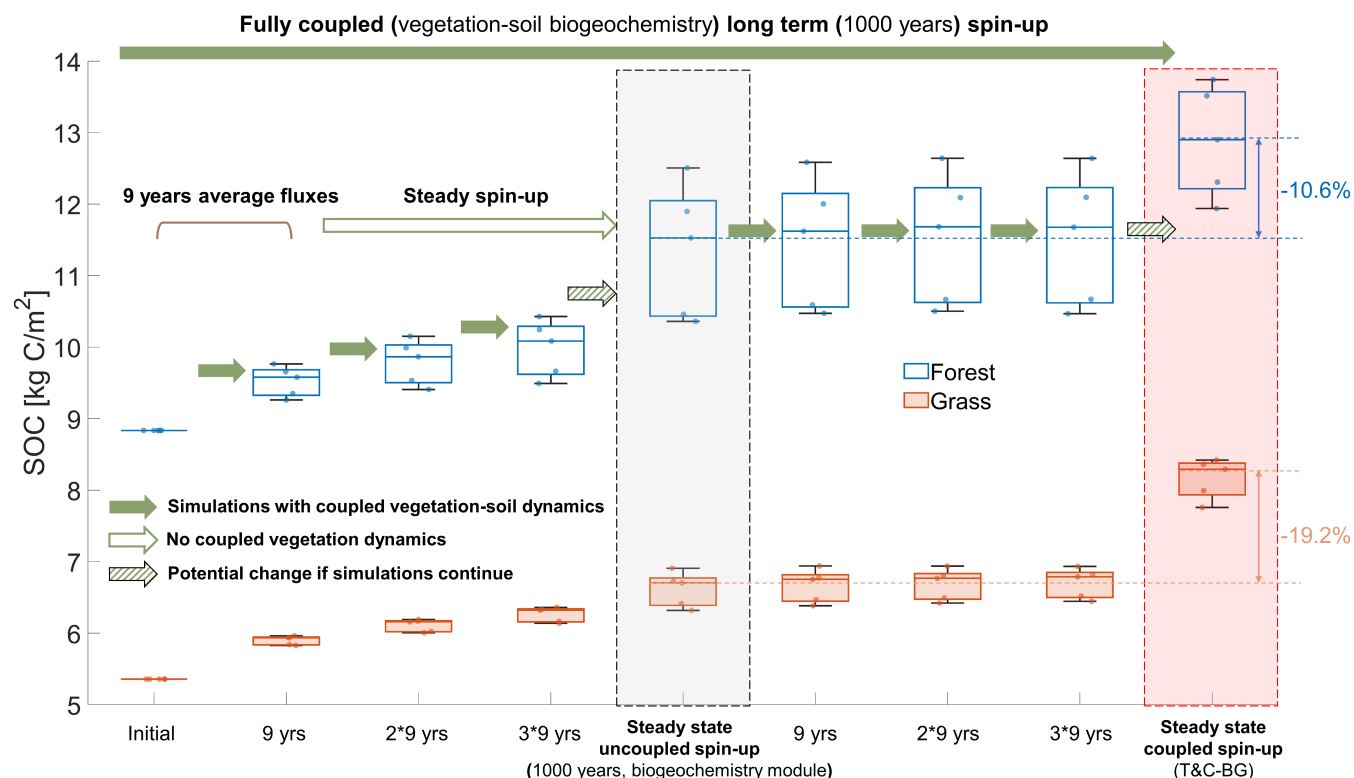
Figure 7. Evolution of soil organic carbon (SOC) during different initialization schemes and simulation durations at 10 selected sites (Fig. 2h). Blue/orange boxplots represent forest/grassland sites. Arrows indicate simulation transitions between stages. The initial values (far left) are followed by 3*9-year simulations using the fully coupled T&C-BG model (solid green arrows). The average vegetation fluxes are extracted from the first 9 years to obtain a steady state condition with the biogeochemistry-only module (outlined green arrow, middle gray box). This is followed by three additional 9-year simulations. A comprehensive long-term spin-up using the fully coupled T&C-BG model (i.e., considering coupled vegetation and soil biogeochemical dynamics) is shown in the right red box. Striped arrows indicate the potential direction of SOC change if coupled simulations continue beyond the current duration.

In summary, the domain used here contains 1859 cells in total. Tracking lateral fluxes in all cells increases computational cost significantly (e.g., by approximately 50% compared to a simulation without tracking any fluxes), whereas tracking only $n = 10\%$ of the cells has less than 10% impact on the overall simulation time. In Erlenbach, SOC requires over 300 years of
350   simulation to reach steady state (Fig. S8) even without coupled vegetation-soil biogeochemical dynamics. The proposed initialization framework reduces this demand by collapsing the full 300-year 2D spin-up into two 9-year simulations (corresponding to Figs. 2b and 2f), combined with a 1D plot-scale spin-up. This results in a computational saving of approximately 90%.

4   Discussion

This study presents a novel initialization scheme for spatially distributed coupled ecohydrological-soil biogeochemical models
that combines a flux-tracking spin-up with a RF algorithm. The core concept is to explicitly account for lateral fluxes through
a 1D flux-tracking approach to obtain steady-state conditions at a subset of representative cells, and then use a RF model to
extrapolate these results across the entire domain. The scheme improves computational efficiency through two key steps: (1) the
1D flux-tracking spin-up, combined with a biogeochemistry-only submodule, enables steady-state estimation using only two
simulations with measured data, while explicitly accounting for lateral exchanges, thereby producing a more realistic steady
state under catchment conditions; and (2) the RF model significantly reduces the number of cells requiring flux tracking. For the
case study here and using the T&C-BG-2D model, this approach reduced computational costs by up to 90%. Using the proposed
initialization scheme, this study further highlights the substantial role of topography in regulating soil-biogeochemical states
across catchments, which needs to be explicitly considered in the initialization of distributed soil biogeochemical models.

Overall, our experiments confirm the four hypotheses outlined in the introduction. Spatially explicit spin-up (H1) is necessary
to capture spatial variability in soil carbon and nutrient pools, while RF-based extrapolation from a subset of representative cells
(H2) provides an efficient and accurate alternative to a fully distributed and computationally expensive spin-up. The required
sampling fraction (H3) is not universal but depends on catchment-specific heterogeneity and the choice of predictors. Finally,
an uncoupled biogeochemistry-only spin-up (H4) offers a computationally efficient first step, yielding steady states sufficiently
close to the fully coupled solution, hence justifying its use in practical applications.

The approach proposed here is not limited to T&C-BG-2D but can be readily applied for the initialization of other spatially
distributed ecohydrological-soil biogeochemical frameworks. Many such models (e.g., RHESSys (Tague and Band, 2004),
Flux-PIHM-BGC (Shi et al., 2018)) couple a hydrological component with a plot-scale vegetation and/or soil biogeochemistry
module. In these systems, lateral transport of water and carbon can be tracked and incorporated into the plot-scale spin-up,
which can then be combined with a RF algorithm to initialize the steady state across the entire catchment.

The Erlenbach catchment was used here as a testbed to evaluate the effectiveness of the new initialization scheme. Results
show that, for this site, tracking only 40% of the cells is sufficient for the RF model to reconstruct over 90% of the spatial
variability in key soil biogeochemical variables. However, this proportion (40%) should not be interpreted as a universal
threshold. Our scenario experiments indicate that the optimal percentage is catchment-dependent and shaped by the degree of
heterogeneity in vegetation, soils, and topography. For instance, in the *Homog. Veg* scenario even 20% of tracked cells was
sufficient, whereas in the *Random Soil* scenario, additional soil predictors were needed to adequately capture SOC variability.
Flatter topographies here did not necessarily reduce the required sample size, both because the contributing area in the two
flatter topographies remains largely unchanged and because heterogeneity of the domain (in soil and vegetation) still needed to
be sufficiently represented in the sampling. Sensitivity analysis suggests that vegetation type is the most important predictor in
the RF model. Taken together, these findings indicate that the sampling fraction required for effective RF initialization may vary
depending on specific catchment characteristics. In particular, it is influenced by the level of heterogeneity in the landscape,

the unevenness of RF predictor distributions, and the number and type of predictors considered (e.g., inclusion of additional soil information or vegetation attributes).

A sensitivity analysis of predictor importance in the RF model indicates that the type of vegetation is the most influential variable (Fig. S9), followed by elevation. This aligns with previous studies showing that vegetation strongly influences the
390 spatial distribution of SOC (e.g., Kunkel et al., 2022; Yao et al., 2023), and that elevation is a dominant control, at least in pronounced topographies such as Erlenbach (Stähli et al., 2021; Lian et al., 2025a). The relative importance of these predictors may vary in catchments with different climatic and topographic characteristics. Note that soil texture is relatively less important in the sensitivity analysis in Fig. S9. This is likely due to the relatively homogeneous soil texture distribution in Erlenbach. However, simulations from the *Random Soil* scenario (Section 3.2) highlight the essential role of including soil information
395 among the RF predictors, particularly in areas characterized by high soil spatial variability.

While the proposed framework performs robustly in our tests, a few aspects deserve special attention and should be considered for applications in specific cases. In this study, the average soil texture was used in step (a) of the initialization procedure (Fig. 2) for the *Random soil* scenario, and the resulting steady-state conditions were assigned to all cells. This simplification may introduce a potential bias, as different soil textures can alter the degree of water limitation experienced by vegetation,
400 thereby affecting plant fluxes and ultimately the initialization outcome. To evaluate this effect, we tested three soil texture settings (sand (60% sand, 10% clay), loam (40.5% sand, 26.5% clay), and clay (20% sand, 50% clay)) in step (a) of Fig. 2, and found that the resulting initialization states and spatial distributions are largely unchanged (see Fig. S10). However, this is likely due to the fact that vegetation in the Erlenbach does not experience water limitation. Conversely, in drier regions, soil texture could become a major constraint and separate spin-ups for each soil type may be required instead of using an average
405 soil texture.

The initialization scheme proposed here provides steady-state initial conditions. This is indeed a convenient simplification (often adopted in soil biogeochemical modeling), which may not always be realistic, especially over long timescales and certain contexts (e.g., long-term vegetation colonization, young forest development, post-disturbance recovery after wildfires (Guo and Gifford, 2002; Ilstedt, 2003; Nave et al., 2011; Zhang et al., 2023)). To apply the proposed approach in systems that
410 are not in steady state, modifications are required. One possible strategy could be to assume a pre-disturbance steady state, derive the initial condition from that point, and then iteratively apply the initialization scheme over shorter time intervals. For example, in an area undergoing young forest growth, the initial condition may be approximated from the land use prior to forest establishment. A short-term simulation (e.g., 1 year) can then be used to obtain average plant fluxes. These fluxes can be applied in a longer simulation period (e.g., 5 years), followed by another short-term run to update the fluxes. This process
415 introduces a loose coupling between vegetation dynamics and soil biogeochemistry, allowing the model to gradually adjust toward a consistent state. The simulation–flux update cycle can be repeated until model outputs align with observations. It is important to note that only the 1D spin-up component of the initialization scheme requires modification in such cases; the RF algorithm remains applicable without change. However, if only part of the catchment is affected by disturbance, separate RF models may be needed for disturbed and undisturbed regions.

5   Conclusions

This study presents a novel initialization scheme for spatially distributed coupled ecohydrological-soil biogeochemical models, integrating a flux-tracking spin-up with a RF algorithm, thus contributing to ongoing efforts in the development and reliable application of fully coupled spatially distributed models. Our results underscore the importance of explicitly accounting for lateral fluxes and spatial heterogeneities in model initialization for accurately reducing biases in modeled patterns of soil carbon and nutrients. The proposed framework achieves a dynamic steady state efficiently and demonstrates robust performance of the RF model, which required tracking lateral fluxes for only a relatively limited number of cells to effectively represent spatial variability in the setup of initial conditions for carbon and nutrient pools. The number of cells required for lateral flux tracking is primarily determined by the spatial complexity of the catchment and the amount of spatial information contained in the predictors used in the RF model. While demonstrated using T&C-BG-2D, the methodology proposed here is broadly applicable to other spatially distributed models, offering an efficient framework to improve the accuracy of distributed soil biogeochemical models by explicitly including spatial information in their spin up and initialization, while maintaining a reasonable computational effort. This will ultimately enhance not only our ability to reproduce spatial patterns of soil carbon and nutrients at the catchment scale but also our understanding of the role of topography in modulating coupled processes related to water, energy, and biogeochemical fluxes in complex landscapes.

Code and data availability.   The T&C model code, including biogeochemistry, can be obtained from Fatichi (2025), while the T&C-BG-2D model code is from Lian et al. (2025a). Catchment meteorological data for Erlenbach can be found in the WSL data portal (Stähli, 2018). The accompanying initialization procedures and setup files can be found on Zenodo (Lian et al., 2025b).

Author contributions.   TL and SB conceived the idea and designed the study. TL carried out the numerical simulations, while ZZ and AP performed additional plot-scale simulations for the fully coupled T&C-BG model. TL and SB analyzed the results. TL drafted the first version of the manuscript, with significant contributions from SB. All authors contributed to the interpretation of the results and the writing of the final version.

Competing interests.   The authors declare that they have no competing interests.

Acknowledgements.   SB and TL acknowledge funding from the Swiss National Science Foundation (SNSF, Grant 10002612).

References

445 Ammann, C., Spirig, C., Leifeld, J., and Neftel, A.: Assessment of the nitrogen and carbon budget of two managed temperate grassland fields, Agriculture, Ecosystems & Environment, 133, 150–162, https://doi.org/10.1016/j.agee.2009.05.006, 2009.

Baroni, G., Schalge, B., Rakovec, O., Kumar, R., Schüler, L., Samaniego, L., Simmer, C., and Attinger, S.: A Comprehensive Distributed Hydrological Modeling Intercomparison to Support Process Representation and Data Collection Strategies, Water Resources Research, 55, 990–1010, https://doi.org/10.1029/2018WR023941, 2019.

450 Botter, M., Zeeman, M., Burlando, P., and Fatichi, S.: Impacts of fertilization on grassland productivity and water quality across the European Alps under current and warming climate: insights from a mechanistic model, Biogeosciences, 18, 1917–1939, https://doi.org/10.5194/bg-18-1917-2021, 2021.

Breiman, L.: Random Forests, Machine Learning, 45, 5–32, https://doi.org/10.1023/A:1010933404324, 2001.

Carranza, C., Nolet, C., Pezij, M., and Van Der Ploeg, M.: Root zone soil moisture estimation with Random Forest, Journal of Hydrology,
455 593, 125 840, https://doi.org/10.1016/j.jhydrol.2020.125840, 2021.

Christensen, L., Tague, C. L., and Baron, J. S.: Spatial patterns of simulated transpiration response to climate variability in a snow dominated mountain ecosystem, Hydrological Processes, 22, 3576–3588, https://doi.org/10.1002/hyp.6961, _eprint: https://onlinelibrary.wiley.com/doi/pdf/10.1002/hyp.6961, 2008.

Fatichi, S.: Tethys-Chloris (T&C) - Terrestrial Biosphere Model – Public release January 2025, https://doi.org/10.24433/CO.0905087.V4,
460 [software], 2025.

Fatichi, S., Ivanov, V. Y., and Caporali, E.: A mechanistic ecohydrological model to investigate complex interactions in cold and warm water-controlled environments: 1. Theoretical framework and plot-scale analysis, Journal of Advances in Modeling Earth Systems, 4, 2011MS000 086, https://doi.org/10.1029/2011MS000086, 2012.

Fatichi, S., Pappas, C., and Ivanov, V. Y.: Modeling plant–water interactions: an ecohydrological overview from the cell to the global scale,
465 WIREs Water, 3, 327–368, https://doi.org/10.1002/wat2.1125, 2016.

Fatichi, S., Manzoni, S., Or, D., and Paschalis, A.: A Mechanistic Model of Microbially Mediated Soil Biogeochemical Processes: A Reality Check, Global Biogeochemical Cycles, 33, 620–648, https://doi.org/10.1029/2018GB006077, 2019.

Guo, L. B. and Gifford, R. M.: Soil carbon stocks and land use change: a meta analysis, Global Change Biology, 8, 345–360, https://doi.org/10.1046/j.1354-1013.2002.00486.x, 2002.

470 Gupta, S., Lehmann, P., Bonetti, S., Papritz, A., and Or, D.: Global Prediction of Soil Saturated Hydraulic Conductivity Using Random Forest in a Covariate-Based GeoTransfer Function (CoGTF) Framework, Journal of Advances in Modeling Earth Systems, 13, e2020MS002 242, https://doi.org/10.1029/2020MS002242, 2021.

Gupta, S., Hasler, J. K., and Alewell, C.: Mining soil data of Switzerland: New maps for soil texture, soil organic carbon, nitrogen, and phosphorus, Geoderma Regional, 36, e00 747, https://doi.org/10.1016/j.geodrs.2023.e00747, 2024.

475 Hashimoto, S., Wattenbach, M., and Smith, P.: A new scheme for initializing process-based ecosystem models by scaling soil carbon pools, Ecological Modelling, 222, 3598–3602, https://doi.org/10.1016/j.ecolmodel.2011.08.011, 2011.

Ilstedt, U.: Changes in soil chemical and microbial properties after a wildfire in a tropical rainforest in Sabah, Malaysia, Soil Biology and Biochemistry, 35, 1071–1078, https://doi.org/10.1016/S0038-0717(03)00152-4, 2003.

Kim, K. B., Kwon, H.-H., and Han, D.: Exploration of warm-up period in conceptual hydrological modelling, Journal of Hydrology, 556,
480 194–210, https://doi.org/10.1016/j.jhydrol.2017.11.015, 2018.

Krinner, G., Viovy, N., De Noblet-Ducoudré, N., Ogée, J., Polcher, J., Friedlingstein, P., Ciais, P., Sitch, S., and Prentice, I. C.: A dynamic global vegetation model for studies of the coupled atmosphere-biosphere system, Global Biogeochemical Cycles, 19, 2003GB002 199, https://doi.org/10.1029/2003GB002199, 2005.

Kunkel, V., Wells, T., and Hancock, G.: Modelling soil organic carbon using vegetation indices across large catchments in eastern Australia, Science of The Total Environment, 817, 152 690, https://doi.org/10.1016/j.scitotenv.2021.152690, 2022.

Li, J., Zhang, D., and Liu, M.: Factors controlling the spatial distribution of soil organic carbon in Daxing'anling Mountain, Scientific Reports, 10, 12 659, https://doi.org/10.1038/s41598-020-69590-y, 2020.

Lian, T., Fatichi, S., Stähli, M., and Bonetti, S.: Assessing Spatial Patterns of Carbon and Nutrient Dynamics in Catchments of Complex Topography, Water Resources Research, 61, e2025WR040 260, https://doi.org/10.1029/2025WR040260, 2025a.

Lian, T., Zhang, Z., Paschalis, A., and Bonetti, S.: TeC_BG_2D_Spin_up: v1.0.0, https://doi.org/10.5281/ZENODO.17213879, [software], 2025b.

Loh, W.-Y.: Regression tress with unbiased variable selection and interaction detection, Statistica sinica, pp. 361–386, publisher: JSTOR, 2002.

Lugato, E., Panagos, P., Bampa, F., Jones, A., and Montanarella, L.: A new baseline of organic carbon stock in European agricultural soils using a modelling approach, Global Change Biology, 20, 313–326, https://doi.org/10.1111/gcb.12292, 2014.

Mahdavi, S., Salehi, B., Granger, J., Amani, M., Brisco, B., and Huang, W.: Remote sensing for wetland classification: a comprehensive review, GIScience & Remote Sensing, 55, 623–658, https://doi.org/10.1080/15481603.2017.1419602, 2018.

Manzoni, S., Schimel, J. P., and Porporato, A.: Responses of soil microbial communities to water stress: results from a meta-analysis, Ecology, 93, 930–938, https://doi.org/10.1890/11-0026.1, _eprint: https://onlinelibrary.wiley.com/doi/pdf/10.1890/11-0026.1, 2012.

Manzoni, S., Schaeffer, S. M., Katul, G., Porporato, A., and Schimel, J. P.: A theoretical analysis of microbial eco-physiological and diffusion limitations to carbon cycling in drying soils, Soil Biology and Biochemistry, 73, 69–83, https://doi.org/10.1016/j.soilbio.2014.02.008, 2014.

Martin, M., Orton, T., Lacarce, E., Meersmans, J., Saby, N., Paroissien, J., Jolivet, C., Boulonne, L., and Arrouays, D.: Evaluation of modelling approaches for predicting the spatial distribution of soil organic carbon stocks at the national scale, Geoderma, 223-225, 97–107, https://doi.org/10.1016/j.geoderma.2014.01.005, 2014.

Martín-López, J. M., Verchot, L. V., Martius, C., and Da Silva, M.: Modeling the Spatial Distribution of Soil Organic Carbon and Carbon Stocks in the Casanare Flooded Savannas of the Colombian Llanos, Wetlands, 43, 65, https://doi.org/10.1007/s13157-023-01705-3, 2023.

Meersmans, J., De Ridder, F., Canters, F., De Baets, S., and Van Molle, M.: A multiple regression approach to assess the spatial distribution of Soil Organic Carbon (SOC) at the regional scale (Flanders, Belgium), Geoderma, 143, 1–13, https://doi.org/10.1016/j.geoderma.2007.08.025, 2008.

Moyano, F. E., Manzoni, S., and Chenu, C.: Responses of soil heterotrophic respiration to moisture availability: An exploration of processes and models, Soil Biology and Biochemistry, 59, 72–85, https://doi.org/10.1016/j.soilbio.2013.01.002, 2013.

Nave, L. E., Vance, E. D., Swanston, C. W., and Curtis, P. S.: Fire effects on temperate forest soil C and N storage, Ecological Applications, 21, 1189–1201, https://doi.org/10.1890/10-0660.1, 2011.

Nemo, Klumpp, K., Coleman, K., Dondini, M., Goulding, K., Hastings, A., Jones, M. B., Leifeld, J., Osborne, B., Saunders, M., Scott, T., Teh, Y. A., and Smith, P.: Soil Organic Carbon (SOC) Equilibrium and Model Initialisation Methods: an Application to the Rothamsted Carbon (RothC) Model, Environmental Modeling & Assessment, 22, 215–229, https://doi.org/10.1007/s10666-016-9536-0, 2017.

Ng, G. C., Bedford, D. R., and Miller, D. M.: A mechanistic modeling and data assimilation framework for Mojave Desert ecohydrology, Water Resources Research, 50, 4662–4685, https://doi.org/10.1002/2014WR015281, 2014.

520 Nigrelli, G., Fratianni, S., Zampollo, A., Turconi, L., and Chiarle, M.: The altitudinal temperature lapse rates applied to high elevation rockfalls studies in the Western European Alps, Theoretical and Applied Climatology, 131, 1479–1491, https://doi.org/10.1007/s00704-017-2066-0, 2018.

Noto, L. V., Ivanov, V. Y., Bras, R. L., and Vivoni, E. R.: Effects of initialization on response of a fully-distributed hydrologic model, Journal of Hydrology, 352, 107–125, https://doi.org/10.1016/j.jhydrol.2007.12.031, 2008.

525 Parras-Alcántara, L., Lozano-García, B., and Galán-Espejo, A.: Soil organic carbon along an altitudinal gradient in the Despeñaperros Natural Park, southern Spain, Solid Earth, 6, 125–134, https://doi.org/10.5194/se-6-125-2015, publisher: Copernicus GmbH, 2015.

Parvizi, Y. and Fatehi, S.: Geospatial digital mapping of soil organic carbon using machine learning and geostatistical methods in different land uses, Scientific Reports, 15, 4449, https://doi.org/10.1038/s41598-025-88062-9, 2025.

Paschalis, A., Bonetti, S., Guo, Y., and Fatichi, S.: On the Uncertainty Induced by Pedotransfer Functions in Terrestrial Biosphere Modeling, 530 Water Resources Research, 58, e2021WR031 871, https://doi.org/10.1029/2021WR031871, 2022.

Pazúr, R., Huber, N., Weber, D., Ginzler, C., and Price, B.: Cropland and grassland map of Switzerland based on Sentinel-2 data, https://doi.org/10.16904/ENVIDAT.205, artwork Size: 36873826 bytes, 46196707 bytes, 22951009 bytes, 21028763 bytes, 12925 bytes, 10103 bytes, 773453532 bytes, 773453532 bytes, 22351282 bytes, 20469824 bytes Pages: 36873826 bytes, 46196707 bytes, 22951009 bytes, 21028763 bytes, 12925 bytes, 10103 bytes, 773453532 bytes, 773453532 bytes, 22351282 bytes, 20469824 bytes, 2021.

535 Peters, J., Baets, B. D., Verhoest, N. E., Samson, R., Degroeve, S., Becker, P. D., and Huybrechts, W.: Random forests as a tool for ecohydrological distribution modelling, Ecological Modelling, 207, 304–318, https://doi.org/10.1016/j.ecolmodel.2007.05.011, 2007.

Qiu, H., Niu, J., Baas, D. G., and Phanikumar, M. S.: An integrated watershed-scale framework to model nitrogen transport and transformations, Science of The Total Environment, 882, 163 348, https://doi.org/10.1016/j.scitotenv.2023.163348, 2023.

Qu, Y., Maksyutov, S., and Zhuang, Q.: Technical Note: An efficient method for accelerating the spin-up process for process-based biogeo-540 chemistry models, Biogeosciences, 15, 3967–3973, https://doi.org/10.5194/bg-15-3967-2018, 2018.

Randerson, J. T., Hoffman, F. M., Thornton, P. E., Mahowald, N. M., Lindsay, K., Lee, Y., Nevison, C. D., Doney, S. C., Bonan, G., Stöckli, R., Covey, C., Running, S. W., and Fung, I. Y.: Systematic assessment of terrestrial biogeochemistry in coupled climate–carbon models, Global Change Biology, 15, 2462–2484, https://doi.org/10.1111/j.1365-2486.2009.01912.x, 2009.

Ruiz, S., Or, D., and Schymanski, S. J.: Soil Penetration by Earthworms and Plant Roots—Mechanical Energetics of Bioturbation of Compacted Soils, PLOS ONE, 10, e0128 914, https://doi.org/10.1371/journal.pone.0128914, 2015.

Schwarz, E., Ghersheen, S., Belyazid, S., and Manzoni, S.: When and why microbial-explicit soil organic carbon models can be unstable, Biogeosciences, 21, 3441–3461, https://doi.org/10.5194/bg-21-3441-2024, 2024.

Seck, A., Welty, C., and Maxwell, R. M.: Spin-up behavior and effects of initial conditions for an integrated hydrologic model, Water Resources Research, 51, 2188–2210, https://doi.org/10.1002/2014WR016371, 2015.

550 Senarath, S. U. S., Ogden, F. L., Downer, C. W., and Sharif, H. O.: On the calibration and verification of two-dimensional, distributed, Hortonian, continuous watershed models, Water Resources Research, 36, 1495–1510, https://doi.org/10.1029/2000WR900039, 2000.

Shi, M., Yang, Z.-L., Lawrence, D. M., Dickinson, R. E., and Subin, Z. M.: Spin-up processes in the Community Land Model version 4 with explicit carbon and nitrogen components, Ecological Modelling, 263, 308–325, https://doi.org/10.1016/j.ecolmodel.2013.04.008, 2013.

Shi, Y., Eissenstat, D. M., He, Y., and Davis, K. J.: Using a spatially-distributed hydrologic biogeochemistry model with a nitrogen
555   transport module to study the spatial variation of carbon processes in a Critical Zone Observatory, Ecological Modelling, 380, 8–21,
https://doi.org/10.1016/j.ecolmodel.2018.04.007, 2018.

Simon, S. M., Glaum, P., and Valdovinos, F. S.: Interpreting random forest analysis of ecological models to move from prediction to expla-
nation, Scientific Reports, 13, 3881, https://doi.org/10.1038/s41598-023-30313-8, 2023.

Stähli, M.: Longterm hydrological observatory alptal (central switzerland), https://doi.org/http://dx.doi.org/10.16904/envidat.380, [data set],
560   2018.

Stähli, M., Seibert, J., Kirchner, J. W., Von Freyberg, J., and Van Meerveld, I.: Hydrological trends and the evolution of catchment research
in the Alptal valley, central Switzerland, Hydrological Processes, 35, e14 113, https://doi.org/10.1002/hyp.14113, 2021.

Tague, C. L. and Band, L. E.: RHESSys: Regional Hydro-Ecologic Simulation System—An Object-Oriented Approach to Spa-
tially Distributed Modeling of Carbon, Water, and Nutrient Cycling, Earth Interactions, 8, 1–42, https://doi.org/10.1175/1087-
565   3562(2004)8<1:RRHSSO>2.0.CO;2, 2004.

Teng, M., Zeng, L., Xiao, W., Huang, Z., Zhou, Z., Yan, Z., and Wang, P.: Spatial variability of soil organic carbon in Three Gorges Reservoir
area, China, Science of The Total Environment, 599-600, 1308–1316, https://doi.org/10.1016/j.scitotenv.2017.05.085, 2017.

Thornton, P., Law, B., Gholz, H. L., Clark, K. L., Falge, E., Ellsworth, D., Goldstein, A., Monson, R., Hollinger, D., Falk, M., Chen, J., and
Sparks, J.: Modeling and measuring the effects of disturbance history and climate on carbon and water budgets in evergreen needleleaf
570   forests, Agricultural and Forest Meteorology, 113, 185–222, https://doi.org/10.1016/S0168-1923(02)00108-9, 2002.

Thornton, P. E. and Rosenbloom, N. A.: Ecosystem model spin-up: Estimating steady state conditions in a coupled terrestrial carbon and
nitrogen cycle model, Ecological Modelling, 189, 25–48, https://doi.org/10.1016/j.ecolmodel.2005.04.008, 2005.

Tyralis, H., Papacharalampous, G., and Langousis, A.: A Brief Review of Random Forests for Water Scientists and Practitioners and Their
Recent History in Water Resources, Water, 11, 910, https://doi.org/10.3390/w11050910, 2019.

575   Xia, J. Y., Luo, Y. Q., Wang, Y.-P., Weng, E. S., and Hararuk, O.: A semi-analytical solution to accelerate spin-up of a coupled carbon and
nitrogen land model to steady state, Geoscientific Model Development, 5, 1259–1271, https://doi.org/10.5194/gmd-5-1259-2012, 2012.

Yan, Z., Bond-Lamberty, B., Todd-Brown, K. E., Bailey, V. L., Li, S., Liu, C., and Liu, C.: A moisture function of soil heterotrophic respiration
that incorporates microscale processes, Nature Communications, 9, 2562, https://doi.org/10.1038/s41467-018-04971-6, publisher: Nature
Publishing Group, 2018.

580   Yao, Y., Dai, Q., Gao, R., Yi, X., Wang, Y., and Hu, Z.: Characteristics and factors influencing soil organic carbon composition by vegetation
type in spoil heaps, Frontiers in Plant Science, 14, 1240 217, https://doi.org/10.3389/fpls.2023.1240217, 2023.

Zeraatpisheh, M., Garosi, Y., Reza Owliaie, H., Ayoubi, S., Taghizadeh-Mehrjardi, R., Scholten, T., and Xu, M.: Improving the spatial pre-
diction of soil organic carbon using environmental covariates selection: A comparison of a group of environmental covariates, CATENA,
208, 105 723, https://doi.org/10.1016/j.catena.2021.105723, 2022.

585   Zhan, X., Xue, Y., and Collatz, G.: An analytical approach for estimating CO2 and heat fluxes over the Amazonian region, Ecological
Modelling, 162, 97–117, https://doi.org/10.1016/S0304-3800(02)00405-2, 2003.

Zhang, W., Li, Y., Zhu, B., Zheng, X., Liu, C., Tang, J., Su, F., Zhang, C., Ju, X., and Deng, J.: A process-oriented hydro-biogeochemical
model enabling simulation of gaseous carbon and nitrogen emissions and hydrologic nitrogen losses from a subtropical catchment, Science
of The Total Environment, 616-617, 305–317, https://doi.org/10.1016/j.scitotenv.2017.09.261, 2018.

590   Zhang, Y., Chen, A., Wang, Z., Wang, X., Lin, Y., and Ye, C.: Soil organic carbon accumulation along a chronosequence of vegetation
colonization on debris flow fans in Southwest China, CATENA, 223, 106 936, https://doi.org/10.1016/j.catena.2023.106936, 2023.

Zhu, M., Feng, Q., Qin, Y., Cao, J., Zhang, M., Liu, W., Deo, R. C., Zhang, C., Li, R., and Li, B.: The role of topography in shaping the spatial patterns of soil organic carbon, CATENA, 176, 296–305, https://doi.org/10.1016/j.catena.2019.01.029, 2019.